Testing High-Frequency Electronic Signals With Reflection-Mode Electroabsorption Modulators

Rory L. Van Tuyl, *Fellow, IEEE*, Gloria E. Höfler, Robert G. Ritter, Todd S. Marshall, *Member, IEEE*, Jintian Zhu, Luca Billia, George M. Clifford, William Gong, and David P. Bour, *Fellow, IEEE*

***Abstract*—Remote testing of microwave signals to 25 GHz and digital signals to 12.5 Gb/s is demonstrated through fiber-optic cables. Reflection-mode electroabsorption modulators are used as high-impedance transducers to measure voltage and inject current. Transducers are imbedded in wafer probes, printed circuit probes and microwave packages for various applications including sensing incident and reflected microwave signals, probing serial data streams on printed circuit boards, probing digital and microwave monolithic integrated circuits, and performing time-domain reflectometry.**

Principal advantages of this technology are that it allows test equipment to be located at large distances from the devices being tested and that broadband signals can be remotely observed with little distortion.

***Index Terms*—Digital measurements, electric variables measurement, electroabsorption, integrated-circuit (IC) measurements, pulse measurements, scattering parameters measurement, time-domain reflectometry, transducer.**

I. Introduction

MICROWAVE AND high-speed digital signals are normally conveyed between test equipment and devices-under-test via a coaxial cable, but the dispersive properties of a coaxial cable can contribute objectionable frequency-dependent loss and broadband waveform distortion over even short cables of less than 1-m length. This paper describes a method for overcoming the coaxial cable problem by using a bidirectional fiber-optic link that employs a reflection-mode electroabsorption modulator as an optical-to-electrical (O-E) and electrical-to-optical (E-O) transducer [1].

The reflection-mode electroabsorption modulator is a miniature opto-electronic chip based on multiquantum-well (MQW) device technology [2]. It linearly converts applied voltage to reflected optical power. It also functions as a photodetector and can thus inject current into a circuit under test. Complete switching from the fully reflective state to fully absorbing state can be accomplished with less than 5 V.

Previous systems for testing electronic signals with optics have been based on reflection-mode electrooptic modulators [3]–[5], which are principally used as electric field sensors. Due to their small size ($<$ 1 mm), these modulators may require thousands of volts for compete switching from the reflective to nonreflective state and are, thus, not sensitive enough for many voltage-sensing applications. (Traveling-wave electrooptic modulators can switch in less than 10 V, but are centimeters in length). In addition, electrooptic transducers are E-O converters only.

In this paper, we describe the reflection-mode electroabsorption modulator, explain how it is used for remote sensing through fiber-optic links, and present experimental results for microwave transducers, high-speed digital and analog probes, and time-domain reflectometry.

II. Reflection-Mode Electroabsorption Modulator

A. Device Description

The reflection-mode electroabsorption modulator (see Fig. 1) is a transducer that reflects light into a single optical fiber in proportion to applied voltage.

By using the reflection mode (instead of the transmission mode commonly used in optical communication devices), each transducer can be accessed with a single optical fiber, thus leaving the opposite end of the transducer chip free for electrical connections. Electroabsorption modulators [2] can be made much smaller than electrooptic modulators and are thus preferred for applications where high electrical input impedance and minimum input capacitance are desired, as in the cases of high-frequency remote probing and sensing. An additional advantage of the reflection mode is that it allows for a double pass of light through the modulation region, thus, for a given absorption efficiency, a reflection modulator has only half the capacitance of a transmission modulator.

Our *reflection-mode electroabsorption modulator* is a waveguide optical device built on a semi-insulating InP substrate. Cleaved facets are coated with antireflection ($\rho \leq 0.002$) and HR ($\rho \geq 0.9$) dielectric films. The active absorption section is a p-i-n diode with an MQW i-region configured as an optical waveguide. The active absorption region is 50-μm long, a length chosen to be just long enough for nearly complete absorption and which has a small intrinsic capacitance (50–70 fF). Since the size of the absorbing region is so small, and because

Manuscript received March 12, 2006; revised August 12, 2006.

R. L. Van Tuyl and T. S. Marshall are with Agilent Technologies, Santa Clara, CA 95051 USA (e-mail: rory_vantuyl@agilent.com).

G. E. Höfler was with Agilent Technologies, Palo Alto, CA 94304 USA. She is now with Argos Technologies, Santa Clara, CA 95051 USA.

R. G. Ritter was with Agilent Technologies, Palo Alto, CA 94304 USA. He is now with Avago Technologies, San Jose, CA 95131 USA.

J. Zhu was with Agilent Technologies, Palo Alto, CA 94304 USA. He is now with the Santur Corporation, Fremont, CA 94538 USA.

L. Billia was with Agilent Technologies, Palo Alto, CA 94304 USA. He is now with Pressac, Turin, Italy.

G. M. Clifford was with Agilent Technologies, Palo Alto, CA 94304 USA. He is now with Gen3 Solar Inc., Hayward, CA 94544 USA.

W. Gong was with Agilent Technologies, Palo Alto, CA 94304 USA. He is now with Pelikan Technologies, Palo Alto, CA 94303 USA.

D. P. Bour was with Agilent Technologies, Palo Alto, CA 94304 USA. He is now with the Bridgelux Inc., Sunnyvale, CA 94089 USA.

Digital Object Identifier 10.1109/TMTT.2006.884668

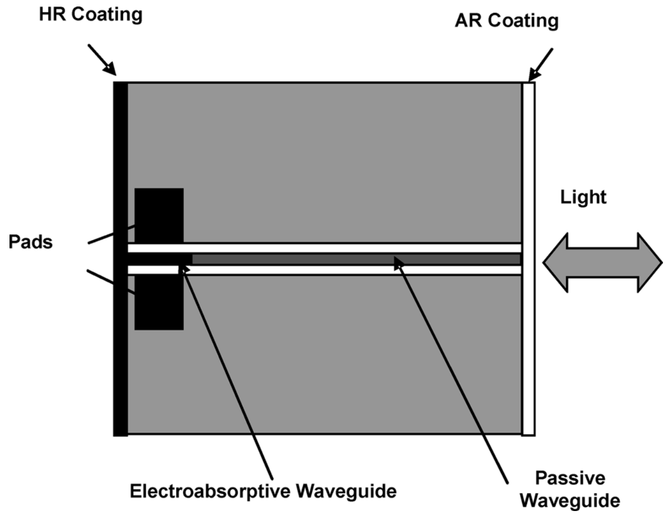

Fig. 1. Top view of reflection-mode electroabsorption modulator chip (300 μm $\times$ 300 μm). Light enters (*right*) through an antireflective (AR) coating, travels through a passive waveguide (250-μm long) to the MQW electroabsorptive waveguide section (50-μm long), reflects from the high reflection (HR) coating to complete a double pass through the quantum-well region, then exits the chip through the passive waveguide. Voltage applied to the pads modulates the absorption of the quantum-well region, causing the reflection coefficient of the modulator to vary with applied voltage.

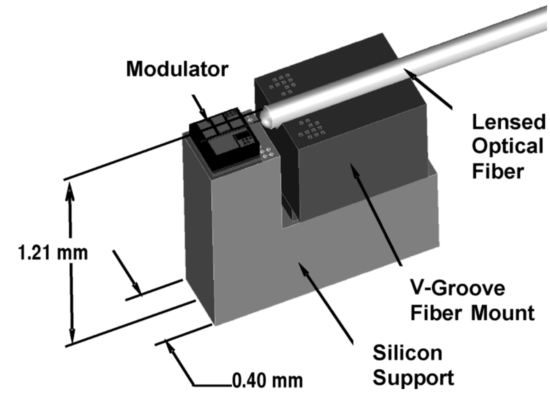

Fig. 2. Drawing of modulator-fiber assembly. A lensed fiber is mounted in a V-groove silicon mount to form a fiber subassembly. The modulator chip is first attached to a silicon submount, then the fiber subassembly is actively aligned using detected current and reflected power as a guide. After alignment, the V-groove fiber mount is attached to the silicon submount.

parts handling demands a chip at least 300 μm$\times$ 300 μm in size, it was necessary to incorporate a passive nonabsorbing waveguide onto the chip to convey light from the input facet to the absorbing region. The input and reflecting facets are 300 μm apart.

Electrical connections to the anode and cathode of the reflection-mode electroabsorption modulator are made through metal pads located near the reflecting facet.

B. Device Material and Process

The active region of the modulator consists of a strain-compensated MQW region composed of nine compressively strained quantum wells with a photoluminescence absorption edge at 1.48 μm. The InGaAsP strained MQW structures and related overgrowths were done in a low-pressure MOVPE reactor with a close-coupled showerhead injector. Trimethyl indium, trimethyl gallium, and triethyl gallium were used for the MQW layers only. Tertiary butylarsine was used for the InGaAsP passive waveguide. Arsine, phosphine, diethyl zinc, and disilane (0.01% in H_2) were used as precursors. An Si-doped InP buffer layer with doping concentration about $n = 1 \times 10^{18}$ cm^{-3} was first deposited to define bias resistors used in the reflection-mode electroabsorption modulator circuits, then followed by growth of the active region. The active region growth was capped with 400 nm of p-type InP.

An SiNx film was deposited and patterned to define the modulator length (50 μm). The p-type InP and the active region around the masked area were removed by inductively coupled plasma etching. With the mask still in place, the passive waveguide layer was formed by selectively growing 0.3-μm InGaAsP (bandgap wavelength $=$ 1.31 μm) covered with undoped InP 0.5-μm thick. To complete the buried heterostructure (BH) lateral waveguide, a 1.5-μm mesa was defined by a standard etching process, and this was followed by selective regrowth of iron-doped InP around the mesa. Once the mask was removed, the 1.5-μm p-type cladding layer and ohmic contact layers were grown. A 3.3-μm-thick polyimide layer was used under the anode bonding pad to minimize parasitic capacitance.

After cleaving rows of devices into bars, high- and low-reflection dielectric coatings are applied to the entrance and reflecting facets. The antireflection coating is a TiO_2 ($n = 2.3$)/SiO_2 ($n = 1.47$) stack with both layers deposited under O_2 rich conditions. Reflectivity is $< 0.2\%$. The high-reflectivity coating is an Si ($n = 3.2$)/SiO_2 ($n = 1.47$) double stack with SiO_2 deposited under O_2 rich conditions. Reflectivity is 94%.

Devices are dc characterized under illumination at this point, and good devices are selected. After final cleaving into chips, the reflection-mode electroabsorption modulators are ready for assembly.

C. Device Assembly

To achieve a low-loss coupling of optical fiber to reflection-mode electroabsorption modulator, a semiautomatic assembly process with machine vision alignment is used. First, the reflection-mode electroabsorption modulator is die-attached to a silicon submount and the polarization-maintaining (PM) fiber is rotationally oriented and attached to an etched V-groove silicon part. Second, the fiber and reflection-mode electroabsorption modulator are actively aligned in three axes using a detected photocurrent and reflected power as alignment indicators. The machine vision system records the relative height and position of fiducial marks for the V-groove and reflection-mode electroabsorption modulator. The two parts are then separated in order to apply solder to the silicon submount for subsequent attachment to the V-groove part. Finally, the two silicon parts are returned to their previously recorded position and soldered together (active alignment is not possible at soldering temperatures). The completed assembly is shown in Fig. 2.

The reflection-mode electroabsorption modulator optical waveguide is nominally 0.3-μm high (Y) and 1.5-μm wide (X). Detected current plotted in an X–Y alignment scan indicates that an elliptical mode approximately 1.1-μm high

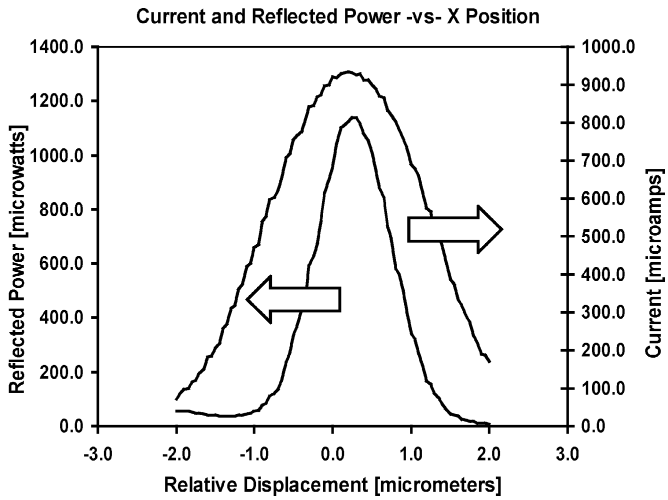

Fig. 3. Detected current and reflected power versus fiber-to-modulator alignment in the horizontal transverse (X) direction. Although the photocurrent collection versus displacement has a 1.25-μm half-width, the reflected power falls to half at only 0.5 μm of misalignment. An alignment tolerance of ± 0.25 μm is required to achieve coupling efficiency equal to 94% of peak.

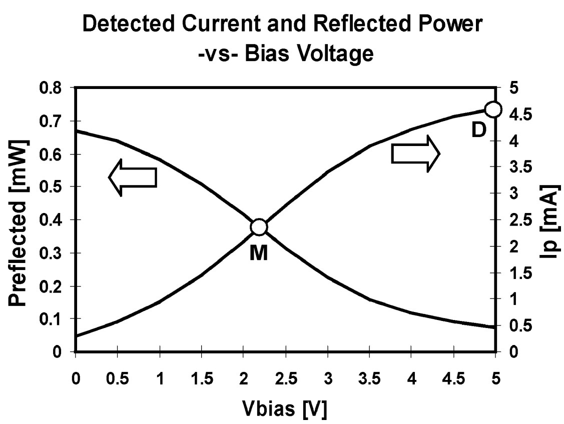

Fig. 4. Reflected power and detected current for modulator-fiber assembly versus voltage applied from modulator cathode to modulator anode. Reflected power slope efficiency (dPr/dV) in this example is 200 μW/V and dynamic conductance is 1.4 mS (714 Ω). Best bias for linear modulator operation is at point M, best bias for photodetection is point D.

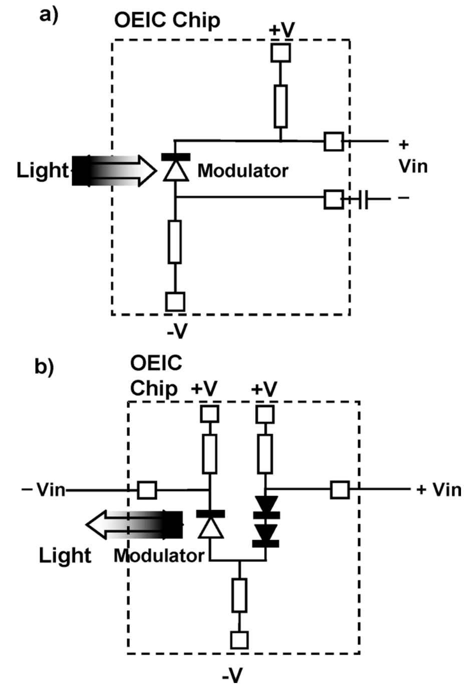

Fig. 5. Schematics of reflection-mode electroabsorption modulator circuit chips used in modulator-fiber assemblies. These simple OEICs are comprised of reflection-mode electroabsorption modulators, resistors, and diodes. Case (a) is a single-ended transducer and case (b) is a dc-coupled differential transducer. For the differential transducer, the required negative anode bias is set by two forward biased diodes connected between $+V\text{in}$ and the modulator's anode. Approximately 2-V bias is generated, allowing the signals $+V\text{in}$ and $-V\text{in}$ to operate at identical average voltages. Reflection-mode electroabsorption modulator OEIC chips are 300 μm $\times$ 450 μm in size.

(Y) and 2.3-μm wide (X) propagates in this waveguide, but similar X–Y scans show that reflected power is collected over a circular area approximately 1 μm in diameter (see Fig. 3). This means that fiber-to-modulator misalignment must be kept to less than ± 0.25 μm to maintain coupling efficiency to within 94% of peak value. We estimate fiber-to-modulator coupling losses to be 1.5–2.2 dB. The externally measured reflection coefficient of the modulator biased to transparency (0 V) is approximately 25% (-6 dB).

D. Reflection and Absorption Characteristics

A plot of typical absorption and reflection characteristics for the reflection-mode electroabsorption modulator is shown in Fig. 4. When biased at point M, the modulator reflects power in linear response to applied signal voltage over a range of approximately 2 V pk-pk. When biased at point D, the modulator acts as a waveguide photodetector with maximum responsivity. Note that at the bias point M, reflected power is reduced to about one-half its maximum value (which is obtained at 0-V bias). Typical reflection coefficients for modulators biased at point M are 0.125. Typical slope efficiency (dPr/dV) for bias at M and incident power of 6.3 mW is 0.7 mW/V.

The bias voltage for linear modulation is sensitive to both device temperature and illumination wavelength. At constant wavelength, the bias voltage for constant reflected power changes by $-24\ \text{mV}/^\circ\text{C}$. To hold reflected power constant over temperature, the illumination wavelength must be changed $+0.4\ \text{nm}/^\circ\text{C}$. For critical applications, the bias point must be stabilized by: 1) holding temperature constant; 2) moving the bias point to hold modulator average current constant; and 3) changing the illumination wavelength to hold modulator current constant.

E. Reflection-Mode Electroabsorption Modulator Opto-Electronic Integrated Circuit (OEIC) Chips

In practice, reflection-mode electroabsorption modulator chips are simple OEICs, as shown in Fig. 5.

Resistors to the negative supply ($-V$) sink the photocurrent required to maintain negative anode bias on the modulator. Resistors connected to the positive supply ($+V$) source current necessary to offset dc current drawn from the signal pads ($+V\text{in}$, $-V\text{in}$) so that no net dc current needs to be supplied by the circuit under test. Inclusion of resistors requires one additional epitaxial layer growth and one additional patterning step. The forward biased diodes are implemented using the same

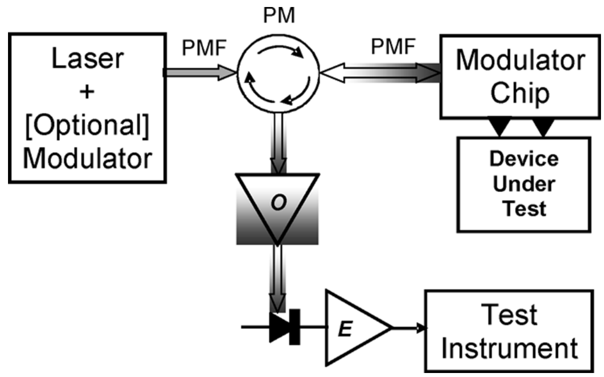

Fig. 6. System for sensing a remote voltage or injecting a remote current with a reflection-mode electroabsorption modulator. CW or modulated light from a laser passes through an optical circulator in PM optical fiber to the modulator. Light is reflected from the modulator in proportion to the voltage presented to it from the device-under-test. This modulated reflected light passes through the optical circulator and an (optional) optical amplifier to a photodetector. The detected photocurrent containing the signal information is amplified by the (optional) electronic amplifier and presented as a voltage to a test instrument.

epitaxial layers and lithography steps as the reflection-mode electroabsorption modulator p-i-n diodes. The OEIC chips are 450 μm $\times$ 300 μm in size.

In operation, the anode of the single-ended device is capacitively coupled to signal ground and the input signal is directly or capacitively coupled to the modulator's cathode. For the differential transducer, the anode and cathode are driven differentially from inputs $+V\text{in}$ and $-V\text{in}$, which can be directly coupled from the device-under-test. Of course, one of the input terminals can be a dc reference voltage if desired.

All results presented here are for the reflection-mode electroabsorption modulator OEIC chips.

III. Sensing System

The reflection-mode electroabsorption modulator transducers are intended for use in the configuration illustrated in Fig. 6.

Light from a 1550-nm distributed feedback (DFB) laser is conveyed via polarization maintaining fibers and an optical circulator to the reflection-mode electroabsorption modulator transducer. If the intention is to inject a signal to the device-under-test, the illuminating light is modulated by an optical modulator following the illuminating laser, and the modulator is biased to 5 V for best detection efficiency and bandwidth. Current is then injected into the device-under-test. Responsivity of the electroabsorption modulator as a photodetector is 0.77 A/W so a modulated power of 6.5 mW supplied to the photodetector produces injected current of 5 mA to the device-under-test.

If, however, the object is to monitor the voltage in the test device, the illumination is continuous wave (CW) light and the modulator is biased to $\sim$ 2 V for best linear modulator operation. Light is reflected from the reflection-mode electroabsorption modulator in linear proportion to the voltage supplied by the device-under-test, and is directed by the PM optical circulator to a photodetector through an (optional) optical amplifier. For most applications, amplification is required, and can be provided by a pre-detection optical amplifier or post-detection electronic amplifier, or both.

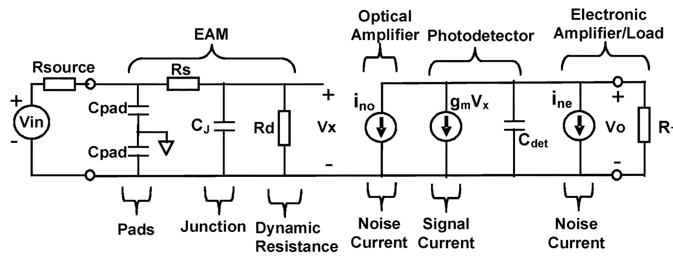

Fig. 7. Linearized electronic circuit model of the modulator-optical amplifier-photodetector link. Modulator and photodetector capacitances form the main bandwidth limitation. The transconductance depends on the modulator slope efficiency, optical amplifier gain, and photodetector responsivity. Voltage gain further depends on load resistance or receiver amplifier transimpedance. Output equivalent noise is generated by a combination of optical and electronic amplifier noise.

TABLE I
Simulated Bandwidth of a Reflection-Mode Electroabsorption Modulator for Various Source Impedances

Source Impedance	Bandwidth[a]
25 Ω	33 GHz
50 Ω	26 GHz
100 Ω	18 GHz

[a]Actual bandwidth is further limited by inductance of the chip-to-signal node interconnection. Photodetection bandwidth [41 GHz] is included in these calculations, but optional transimpedance amplifier bandwidth is not.

For voltage monitoring, it is useful to consider the transfer function of the system from the modulator input terminals to the photodetector output. The resulting low-frequency transconductance is given in (1) as follows:

$$\left(\frac{dip}{dV\text{in}}\right) = gm = \left(\frac{dP}{dV\text{in}}\right) \times G\text{opt} \times r \qquad (1)$$

where

ip	photodetector output current;
P	power reflected from modulator;
$V\text{in}$	input voltage to modulator;
$G\text{opt}$	gain of optical amplifier;
r	responsivity of photodetector (A/W).

The output current is then converted to voltage though a load resistor or transimpedance amplifier.

Operation of the sensing system can be visualized using the electronic equivalent circuit of Fig. 7.

System bandwidth is limited by the chip input capacitances and the source impedance of the test node, as well as the photodetector bandwidth.

For typical measured values of 70-fF modulator junction capacitance and 15-fF pad capacitance, and using a reflection-mode electroabsorption modulator as photodetector operating into a 50-Ω load, theoretical link bandwidths (in the absence of connection inductance) are shown in Table I.

The overall link transfer function, ignoring the frequency response, is given by (2) as follows:

$$\frac{Vo}{Vi} \cong gm \times R_T \qquad (2)$$

TABLE II
PROPERTIES OF UNITY GAIN LINKS WITH OPTICAL AMPLIFIER OR ELECTRONIC TRANSIMPEDANCE AMPLIFIER

Amplifier:	Vo/Vi	Gopt[a]	R_T[b]	E.N.V.[c]	Excess Noise
Optical	1	17 dB	50 Ω	53 nV/√Hz	36 dB
Electronic	1	0 dB	2.4k Ω	42 nV/√Hz	33.4 dB

[a]Optical Amplifier Gain [b]Amplifier Transimpedance
[c]Equivalent input noise voltage spectral density [nV/√Hz]
Calcualations assume: (Modulator slope efficiency=0.6 mW/V; detector responsivity=0.7 A/W; i_{ne}= 15 pA/√Hz; i_{no}=1 nA/√Hz).

TABLE III
CALCULATED REFLECTION-MODE ELECTORABSORPTION MODULATOR DYNAMIC RANGE BASED ON MEASURED NOISE AND DISTORTION

Bandwidth	Noise	Dynamic Range[a]
10 Hz	-122.5 dBm/Hz	132.5 dB
10 kHz	-92.5 dBm/Hz	102.5 dB
10 MHz	-62.5 dBm/Hz	72.5 dB
10 GHz	-32.5 dBm/Hz	42.5 dB

[a] +10dBm maximum signal level (which generates third harmonic distortion less than 30dBc) is assumed.

and the equivalent noise input voltage is (3) as follows:

$$\text{E.N.V.} \cong \frac{((i_{no})^2 + (i_{ne})^2)^{0.5} \times (\Delta f)^{0.5}}{gm} \tag{3}$$

where

Δf noise bandwidth of link;

ino detected optical noise current (A/$\sqrt{}$Hz);

ine electrical noise current (A/$\sqrt{}$Hz).

From (2) and (3), we calculate the required optical or electronic gain required to realize a link gain $= 1$.

The voltage-sensing link cited in Table II has a voltage gain of -34 dB so, in practice, an amplifier is required. A transimpedance amplifier is the preferred receiver for digital signals, and for analog signals where the distortion is not a factor. However, transimpedance amplifiers add distortion and limit the bandwidth of the link to less than could be achieved with an optical amplifier and detector operating directly into a load resistor. Erbium-doped fiber amplifiers were used in this study because they have lower noise than semiconductor optical amplifiers and feature essentially infinite signal bandwidth and zero signal distortion.

When optimally biased at point M (see Fig. 4), distortion due to the modulator's nonlinear transfer characteristic is dominated by third harmonic distortion, which is typically below -30 dBc at $+10$ dBm (2 V pk-pk). Taking $+10$ dBm as the maximum signal limit, link dynamic range for various bandwidths can be read from Table III.

IV. PROBES AND TRANSDUCERS

Operation of reflection-mode electroabsorption modulator transducers has been demonstrated in several configurations, as will be outlined here.

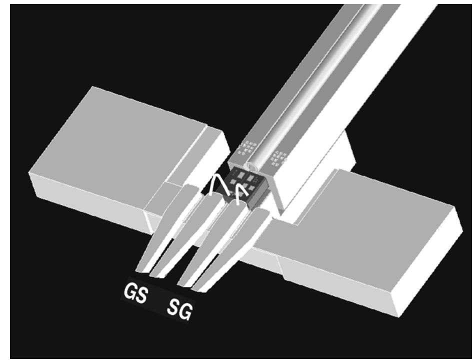

Fig. 8. Drawing of fiber-modulator subassembly mounted with Be–Cu probe tips as part of an IC wafer probe. Probe arrangement fits a particular monolithic IC pad configuration. Inductance associated with the 1-mm-long probe tips produces a significant bandwidth constraint. View is from bottom side of the probe.

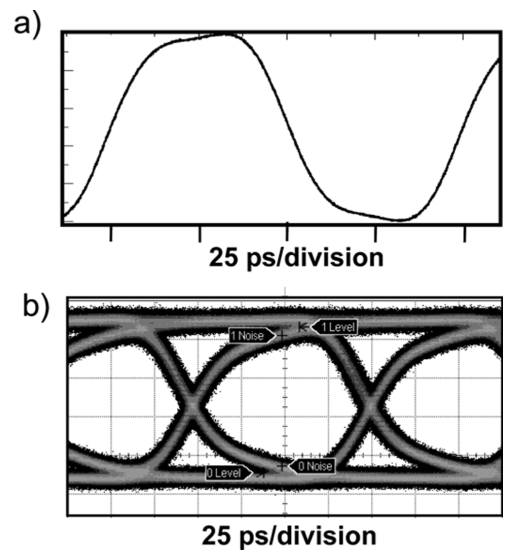

Fig. 9. (a) 10-Gb/s 1010 output of a monolithic IC measured with single-ended OEIC probe (20%/80% rise time $= 26.4$ ps, fall time $= 28.8$ ps, amplitude $= 400$ mV pk-pk, trace taken with 64 averages). Estimated probe rise time is 11 ps. (b) 10-Gb/s pseudorandom bit sequence (PRBS) eye diagram of 800-mV pk-pk differential output IC measured with differential OEIC probe.

A. Wafer Probe

High-impedance probing of integrated circuits (ICs) is accomplished with the reflection-mode electroabsorption modulator probe shown in Fig. 8.

The IC probe combines a modulator-fiber assembly with four Be–Cu probe tips soldered to a sapphire substrate. The probes are 1-mm long and have a 150-μm pitch. DC-bias wires and PM fiber enter the assembly through a mounting fixture attached to a wafer probe station. The relatively large physical size of the probe tips creates a series resonance at 32 GHz in conjunction with the modulator's capacitance. The estimated rise time of the optical probing system is 11 ps. Fidelity of the optically measured pulses compared to the same pulses measured electrically in a 50-GHz bandwidth is excellent. With optical amplification, the link faithfully renders 10-Gb/s waveforms (see Fig. 9).

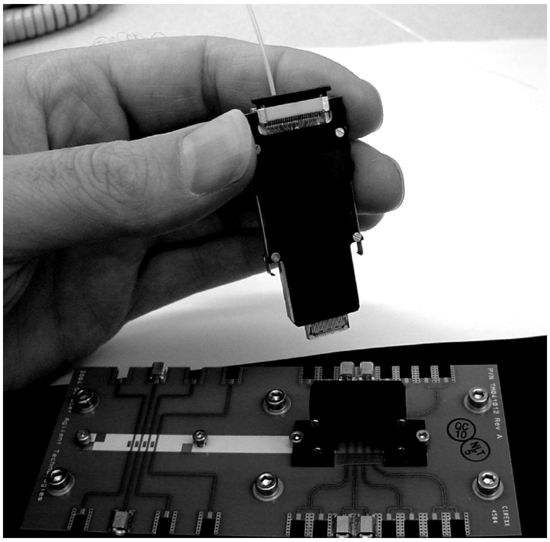

Fig. 10. Printed circuit board probe snaps into retention fixture to contact differential transmission lines on the printed circuit board. Probe tips are 0.75-mm long with 0.414-mm pitch. Contact compliance is furnished by unidirectionally conductive polymer film. Differential reflection-mode electroabsorption modulator chip is used.

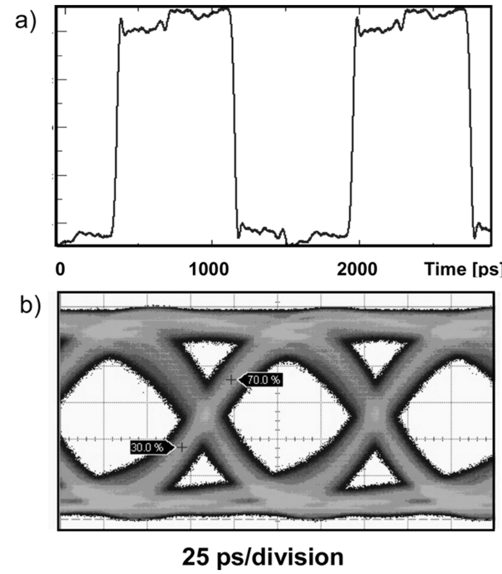

Fig. 11. Waveforms measured with a differential reflection-mode electroabsorption modulator printed circuit board probe. Receiver is a p-i-n detector with transimpedance amplifier (7-GHz bandwidth). No optical amplification was used in the link. In (a), electrical signal reflections are clearly visible on top and base of pulses, revealing impedance mismatches on the printed circuit board. In (b), an open 10-Gb/s PRBS eye diagram is displayed.

B. Printed Circuit Board Probe

To probe 10-Gb/s differential signals on a printed circuit board, we use the differential OEIC mounted in the fixture of Fig. 10.

The modulator-fiber assemblies are connected to a sapphire substrate with 0.75-mm-long probe traces of plated gold. The probe traces contact to the printed circuit board through a sheet of unidirectionally conducting polymer. The probes align to the printed circuit board traces with the aid of an alignment fixture mounted to the printed circuit board. The probe snaps into the alignment fixture to connect to a differential transmission line (356-μm-wide traces on 482-μm pitch).

The printed circuit board probe link used electronic amplification only in the form of a commercial p-i-n transimpedance amplifier module ($r = 1$ A/W, $R_T = 1200\ \Omega$, $\Delta f = 7$ GHz).

The optical probe performs a type of time-domain reflectometry when the printed circuit board traces are driven with wide pulses. Impedance discontinuities and other reflections are clearly visible to the optical probe, as seen in Fig. 11(a). A clean 10-Gb/s eye diagram consistent with the receiver bandwidth is observed in Fig. 11(b).

C. Time-Domain Reflectometry

The reflection-mode electroabsorption modulator transducer can be used to view electrical reflections on transmission lines, as shown in Fig. 11(a). However, it is also possible to inject step inputs to electrical transmission lines using the modulator in the photodetector mode. In this case, an external optical modulator driven by a step generator produces a step increase in optical power at the detector. Fig. 12(a) shows an optically generated step with 17.2-ps rise time, as viewed with a 50-GHz bandwidth electronic sampler. This optical step generation was combined with optical sensing using two reflection-mode electroabsorption modulator transducers to both generate steps and measure electrical reflections [see Fig. 12(b)]. One advantage of these transducers is their ability to inject and measure signals on differential transmission lines.

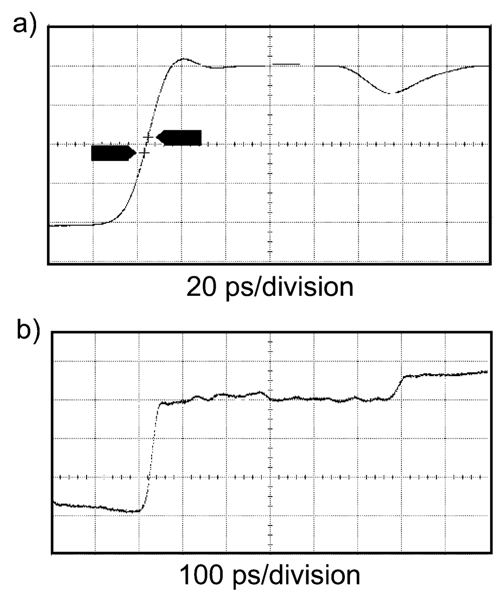

Fig. 12. Time-domain reflectometry. (a) Using the modulator in detector mode, a step current is injected onto a 50-Ω microstrip line. As observed with a 50-GHz bandwidth electrical sampler, the rise time is 17.2 ps, overshoot is 5%, and a capacitive reflection of 18% is observed from a nearby discontinuity. In (b), the step is observed with a nearby reflection-mode electroabsorption modulator transducer, which shows multiple reflections with 26-ps rise time, including a 21% impedance step mismatch.

D. Microwave Transducer

A microwave-sensing link consisting of a 50-Ω terminated reflection-mode electroabsorption modulator input, an optical

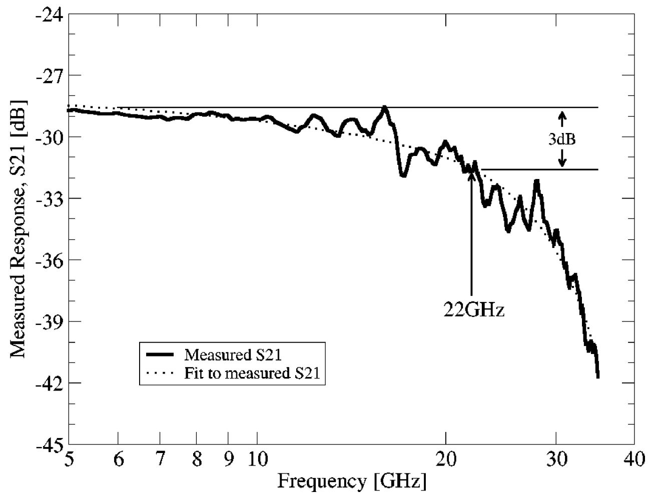

Fig. 13. Measured frequency response of a reflection-mode electroabsorption modulator transducer link. Transducer gain ($S21$) is shown for a transducer in a 50-Ω terminated fixture (effective source impedance driving the modulator is 25 Ω). Rolloff in frequency response below 30 GHz is mainly due to the 25-GHz bandwidth photodetector.

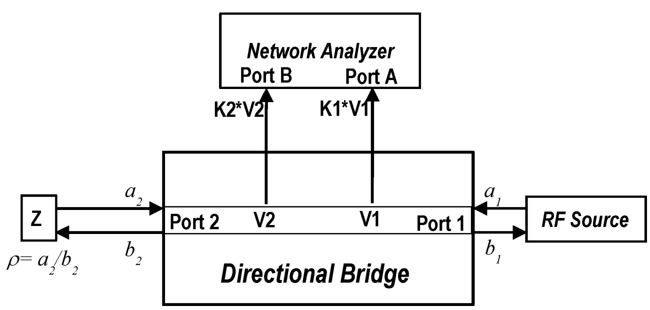

Fig. 14. Directional bridge with reflection-mode electroabsorption modulator voltage sensors. By measuring RF voltage magnitudes and phase difference at two points on the through line, we can compute incident and reflected RF power and, thus, S-parameters. Calibration of the directional bridge with short, open, and load allows for measurement of the reflection coefficient ρ for a test device by a network analyzer located far from the device-under-test. (After [6].)

amplifier, 16 m of optical fiber, and a 50-Ω terminated photodetector ($r = 0.45$ A/W, BW $\sim$ 25 GHz) was constructed. Fig. 13 shows the $S21$ frequency response of this link. The measured bandwidth is 22 GHz and the link gain is -28.5 dB. From package $S11$ measurements, it is inferred that the bandwidth due to capacitive loading by the transducer is > 35 GHz. Additional frequency response rolloff below 30 GHz is attributable to the photodetector.

Equivalent input noise voltage due to the optical amplifier is 60.2 nV/$\sqrt{\text{Hz}}$ (-131.4 dBm/Hz), which is 39.4 dB in excess of the thermal noise of a terminated 50-Ω source.

E. Microwave Directional Bridge

Since the reflection-mode electroabsorption modulator transducers can measure voltage at closely spaced points on a transmission line, it is possible to compute directional power flow and S-parameters of remote loads from these vector voltage measurements (see Fig. 14) [6].

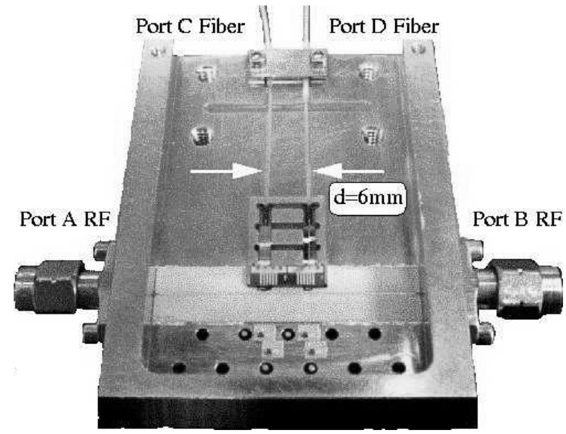

Fig. 15. Microwave directional bridge built with two optical modulator voltage sensors attached to a 50-Ω microstrip transmission through line. Transducers are located 6 mm apart. (From [6].)

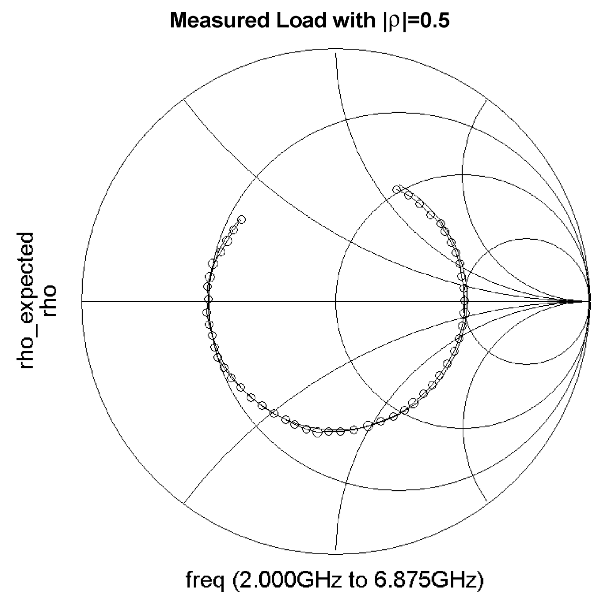

Fig. 16. $S11$ of $\rho = 0.5$ network measured directly with a network analyzer (solid line) and remotely by a network analyzer through a reflection-mode electroabsorption modulator directional bridge (circles). Remote measurement is accurate from 2.0 to 6.9 GHz. (From [6].)

It can be shown [6] that

$$\rho = \frac{a_2}{b_2} = \frac{c_2 \cdot \chi_z - c_0}{1 - c_1 \cdot \chi_z} \tag{4}$$

where

$$\chi_z = \frac{K2 \cdot V2}{K1 \cdot V1} \tag{5}$$

and

$c_0, c_1, c_2 =$ constants determined by calibration procedure.

In situ calibration with short, open, and load standards determines the constants c_0, c_1, and c_2, making it possible to measure the reflection coefficient of an arbitrary load impedance [6]. This depends, however, on $V2$ and $V1$ being independent of one another, a condition that is not met when the separation between the points where they are measured is equal to zero or to an integral number of half-wavelengths of the test frequency. Thus, the spacing between transducers determines the minimum and maximum useful frequencies of operation.

A reflection-mode electroabsorption modulator microwave directional bridge was built in the form of a hybrid microcircuit, as shown in Fig. 15. For this device, the distance between transducers was 6 mm, and measurements could be taken from 0.5 to 9.5 GHz with best accuracy from 2 to 6.9 GHz.

Accurate measurements of the reflection coefficient of a remote impedance were made from 2 to 6.9 GHz with this device. A measurement of $S11$ for a load with reflection coefficient magnitude of 0.5 is shown in Fig. 16.

The microwave directional bridge can, in principle, be extended to higher frequencies by reducing the spacing between transducers.

V. Conclusion

Practical sensors and probes made with reflection-mode electroabsorption modulator OEICs have been used in bidirectional high-frequency connections over optical fiber. Demonstrated applications included monitoring of microwave signals in coaxial cable, probing of 10-Gb/s data on printed circuit boards and ICs, and time-domain reflectometry of microstrip substrates and connectors. Future applications could include remote monitoring and test of electronic and microwave systems and diagnostic testing of electronic equipment via imbedded probes.

Acknowledgment

The authors would like to thank the following Agilent Technologies colleagues for thier contributions to this project: S. Song and J. Norman, for fabrication and assembly, M. Powers for mechanical subassembly development, and S. Newton and W. Ishak for much appreciated management support.

References

[1] R. L. Van Tuyl, "Device for remotely stimulating and measuring electronic signals through a fiber optic cable," U.S. Patent 20050185246, Aug. 25, 2005.

[2] G. L. Li and P. K. L. Yu, "Optical intensity modulators for digital and analog applications," *J. Lightw. Technol.*, vol. 21, no. 9, pp. 2010–2030, Sep. 2003.

[3] J. Valdmanis and G. Mourou, "Subpicosecond electrooptic sampling: Principles and applications," *IEEE J. Quantum Electron.*, vol. QE-22, pp. 69–78, Jan. 1986.

[4] B. Kolner and D. Bloom, "Electrooptic sampling in GaAs integrated circuits," *IEEE J. Quantum Electron.*, vol. QE-22, pp. 79–93, Jan. 1986.

[5] K. Yang, L. P. B. Katehi, and J. F. Whitaker, "Electric field mapping system using an optical-fiber-based electrooptic probe," *IEEE Microw. Wireless Compon. Lett.*, vol. 11, pp. 164–166, Apr. 2001.

[6] T. S. Marshall and R. L. Van Tuyl, "A calibrated microwave directional bridge for remote network analysis through optical fiber," in *IEEE MTT-S Int. Microw. Symp. Dig.*, San Francisco, CA, Jun. 11–16, 2006, ThPK-2.

Rory L. Van Tuyl (SM'77–F'94) received the B.S. and M.S. degrees in electrical engineering from the University of California at Berkeley, in 1965 and 1969, respectively.

In 1969, he joined Hewlett-Packard (now Agilent Technologies), Palo Alto, CA, where he has been involved with microwave and high-speed digital IC design, III–V technology, as well as microwave and lightwave test instrumentation. In 1981, he and his group also reported the first production process for GaAs ICs. From 1988 to 1989, he was a Hewlett-Packard visiting faculty member with the University of California at Santa Barbara. He is currently an Engineer with Agilent Laboratories, Santa Clara CA, where he conducts research in the field of high-frequency test.

Dr. Van Tuyl was the recipient of the 1980 Outstanding Contributed Paper Award presented at the International Solid State Circuits Conference for his paper entitled "A Monolithic GaAs IC Signal Generation Chip."

Gloria E. Höfler received the Ph.D., M.S., and B.S. degrees in electrical engineering from the University of Illinois at Urbana-Champaign, in 1993, 1989, and 1986, respectively.

From 1992 to 1994, she was with the 3M Photonics Laboratory, where she was involved in the development of II–VI blue-green lasers. From 1994 to 2001, she has held various engineering and managerial positions with Hewlett-Packard and Lumileds in the area of III–V opto-electronics ranging from device design and fabrication to packaging. In 2001, she joined Agilent Technologies, Palo Alto, CA, where she was involved with the development of high-speed components for datacom, metro networks, and sensing applications. She is currently with Argos Technologies, Santa Clara, CA. She has authored or coauthored over 40 peer-reviewed publications. She holds several patents.

Robert G. Ritter received the Masters of Science degree in mechanical engineering from the University of California at Berkeley, in 1970.

In 1970, he joined Hewlett-Packard (now Agilent Technologies), Palo Alto, CA, where he was involved with the company's first disc drive. He was involved with several other disc drive projects and was a Project Manager for the mechanical design of the first "Winchester" technology drive in Hewlett-Packard. In 1979, he transferred to Hewlett-Packard Laboratories, where he was involved with the "moving paper" plotter project, robotic mechanisms, and robotic systems. He also contributed to modeling and simulation software for manufacturing systems and supply chains. In 1996, he became a Project Manager for automation technologies, where he has overseen development and transfer to production of several manufacturing automation systems. He is currently with Avago Technologies, San Jose, CA.

Mr. Ritter is a member of the Society of Manufacturing Engineers/Robotics International and the Society of Photo-Optical Instrumentation Engineers.

Todd S. Marshall (S'97–M'00) received the B.S. degree in engineering physics, M.S. degree in electrical engineering, and Ph.D. degree in electrical engineering from the University of Colorado at Boulder, in 1992, 1996, and 2000, respectively.

From 1992 to 1995, he was contracted by the National Renewable Energy Laboratory, Golden CO, to develop and implement computational models of textured solar cell light-trapping effects for efficiency optimization. In 2000, he joined Agilent Technologies, where he was involved with microwave design for 40-Gb/s test equipment. He is currently an Engineer with Agilent Laboratories, Santa Clara, CA, where he conducts research in the field of high-frequency testing. His research interests also include full-wave electromagnetic modeling and open GL visualization.

Jintian Zhu received the B.S. degree in semiconductor physics, M.S. degree in semiconductor device physics and Ph.D. degree in opto-electronics (1994) from Jilin University, Changchun, China, in 1986, 1989, and 1994, respectively.

From 1994 to 1998, he was a Post-Doctoral Researcher with the University of California at San Diego, La Jolla, where he performed research on material growth by MOCVD for high-speed modulators. From September 1998 to October 1999, he was involved with material growth for opto-electronic devices with Multiplex Inc. In 1999, he joined Agilent Technologies, Palo Alto, CA, where he was involved with material growth and device design for various

opto-electronic devices and OEICs, including the reflection-mode electroabsorption modulator. He is currently a Senior Member of Technical Staff with the Santur Corporation, Freemont, CA, where he conducts research on tunable DFB lasers.

Luca Billia received the M.S. degree in electrical engineering from the Politecnico di Torino, Turin, Italy, in 2002.

From 2002 to 2004, he was with Agilent Technologies, Palo Alto, CA, and Turin Italy. He is currently with Pressac, Turin, Italy.

George M. Clifford received the B.S. and M.S. degrees in mechanical engineering from the University of California at Berkeley, in 1967 and 1971, respectively.

In 1971, he joined Hewlett-Packard (now Agilent Technologies), Palo Alto, CA, where he has been involved with mechanical development for spectrometry, magnetic printing, moving paper plotting, magnetic recording, magnetooptic recording, and precision assembly. He is currently with Gen3 Solar Inc., Hayward, CA.

William Gong received the B.S. degree in electrical engineering from Cooper Union, New York City, NY, in 1971, and the M.S.E.E. degree from Columbia University, New York, NY, in 1973.

He was with the IBM Corporation, where he was involved with computer simulation of nMOS circuits in large-scale integration (LSI) chips. He was also with PMI Motors Inc., where he designed motor controllers and optical encoders, and served as an Applications Engineer. In 1977, he joined Hewlett-Packard (now Agilent Technologies), Palo Alto, CA, where he was involved in analog circuit design of power supplies and data-acquisition products, robotics, and precision assembly research and development. He is currently with Pelikan Technologies, Palo Alto, CA.

David P. Bour (S'83–M'84–SM'88–F'00) received the B.S. degree in physics from the Massachusetts Institute of Technology (MIT), Cambridge, in 1983, and the Ph.D. degree in electrical engineering from Cornell University, Ithaca, NY, in 1987.

From 1987 to 1991, he was a Member of Technical Staff with the Sarnoff Corporation. From 1991 to 1999, he was a Principal Scientist with the Electronic Materials Laboratory, Palo Alto Research Center, Xerox, Palo Alto, CA, where he fabricated nitride blue laser diodes and phosphide red laser diodes for laser printing. From 1999 to 2005, he was an Agilent Fellow with the Photonics and Electronics Research Laboratory, Agilent Laboratories, Palo Alto, CA, where he was involved with lasers for communication, data storage and display, and electroabsorption modulators. He is currently with Bridgelux Inc., Sunnyvale, CA. He has authored or coauthored over 200 papers and several book chapters. He holds over 50 U.S. patents.